Journal of Solid State Chemistry 182 (2009) 3085–3090

Contents lists available at ScienceDirect

Journal of Solid State Chemistry

journal homepage: www.elsevier.com/locate/jssc

High pressure induced coordination evolution in chain compound Li_2CuO_2

Shujie You [a], Zhi Li [a], Liuxiang Yang [a], Cheng Dong [a], Liangcheng Chen [a], Changqing Jin [a,*], Jingzhu Hu [b], Guoyin Shen [c], Hokwang Mao [c]

[a] Institute of Physics, Chinese Academy of Sciences, P.O. Box 603, Beijing 100190, PR China
[b] National Synchrotron Light Source, Brookhaven National Lab, Uptown, USA
[c] HPCAT, Geophysical Laboratory, Carnegie Institution of Washington, Argonne, USA

ARTICLE INFO

Article history:
Received 8 May 2009
Received in revised form
16 August 2009
Accepted 19 August 2009
Available online 27 August 2009

Keywords:
Li_2CuO_2
CuO_2 chain
High pressure
Crystal structure

ABSTRACT

Using diamond anvil cell technique with angle dispersive X-ray diffraction (ADXD) of synchrotron radiation and electrical conductivity measurements, we have observed that CuO_2 chain compound Li_2CuO_2 transforms from ambient orthorhombic symmetry into a new phase at above 5.4 GPa and room temperature. The new phase was found to be of monoclinic structure with an increased oxygen coordination number of Cu^{2+} from four at ambient to six at high pressure that provides a structural basis of the evolution of principle physical properties. The high pressure phase of Li_2CuO_2 is discussed in line with the first principle calculations.

1. Introduction

It has been well established that pressure induces a coordination change from four to six in silicate [1]. This coordination change is very important to understand the mineral chemistry of mantle region of the Earth. Copper oxides have been becoming increasingly important since the discovery of high Tc superconductivity (HTS) in cuprates where the CuO_2 plane with four-square coordination plays significant role in supporting supercurrent. One of mysterious for HTS is that the superconducting transition temperatures (Tc) increase with pressure for almost all HTS, while pressure induced superconductivity was discovered in the $Sr_{14}Cu_{24}O_{41}$ chain ladder compound [2,3]. Therefore studies of pressure tuned crystal structure of four square coordinated low dimensional copper oxides are essential to understand the unusual physics properties of cuprates under pressure. Li_2CuO_2 is a typical one-dimensional (1-D) cuprate composed by a series of edge-sharing CuO_4 squares as shown in Fig. 1. These parallel infinite CuO_2 chains are connected by LiO_4 tetrahedra between them. As a potential high-Tc superconductor, Li_2CuO_2 has been widely investigated ranging from theoretical modeling or calculations [4–6] to experimental investigations [7–9] on electronic and magnetic properties. Li_2CuO_2 crystallizes into an orthorhombic structure with space group *Immm* at ambient pressure [5,10], as shown in Fig. 1. The crystal structure is featured with the edge-sharing [CuO_4] planar units that lie in the (*b*, *c*) plane and align along the *b* direction. The Cu–O–Cu bond angle θ is about 94° [10], which is smaller than other typical edge-sharing 1-D cuprates, for example, $CuGeO_3$ which has θ equal to 99° [11]. According to Goodenough, Kanamori and Anderson [12–14], the M–O–M (where M is a transition metal) bond angle plays a substantial role in shaping the magnetism of strongly correlated transition metal oxides. The exchange interaction parameter *J* will change from positive to negative as the M–O–M bond angle crosses a critical value of 90°, corresponding to ferromagnetic (FM) and anti-ferromagnetic (AFM) ordering, respectively. For Li_2CuO_2, it turned out to be a charge transfer insulator with FM nearest neighbor interaction ($J_1 < 0$) and AFM next nearest neighbor interaction ($J_2 > 0$) [5].

Another remarkable feature of Li_2CuO_2 is its simple inter-chain structure: the chains are just parallel to each other. Other 1-D cuprates have more complex inter-chain structures. For example, $GeCuO_3$ has its Cu–O chains tilted about 60° [8], $La_6Ca_8Cu_{24}O_{41}$ has both chains and ladders [15]. The parallel chains make Li_2CuO_2 a more suitable model for studying the simple CuO_2 chain properties. It is paramagnetic at room temperature while an antiferromagnetic (AFM) ordering emerges at 9 K [16,17]. The magnetic structure below T_N is FM along *a* (perpendicular to the CuO_4 plaque) and *b* axes while AFM along *c* axis [18]. However, an NMR study by Li^7 showed that inter-chain interaction dominants in Li_2CuO_2 [19], which indicated that its electron structure is complex in its simple crystal structure.

The behaviors of compounds under high pressure like the chain compound $CuGeO_3$ have been extensively investigated since

* Corresponding author. Fax: +86 10 82649531.
E-mail address: jin@aphy.iphy.ac.cn (C. Jin).

0022-4596/$ - see front matter © 2009 Elsevier Inc. All rights reserved.
doi:10.1016/j.jssc.2009.08.019

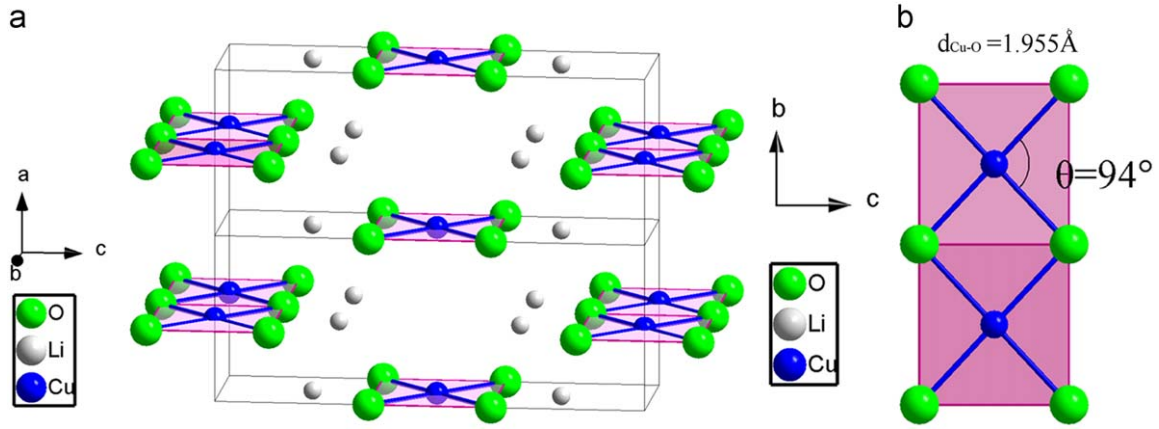

Fig. 1. Schematic view of the orthorhombic Li_2CuO_2 (ambient or phase I).

pressure is very effective to modulate dimensionality and thus to physical properties. For example, as the first known inorganic material that has spin–Peierls (SP) transition, the SP temperature of $CuGeO_3$ increases strongly as pressure increases [23]; three structure transitions were observed in $CuGeO_3$ at room temperature from ambient pressure to 42 GPa with different hydrostatic conditions [20–22]; the high pressure phases of $CuGeO_3$ differ from each other by color coordination of Ge^{4+} and Cu^{2+} ions and the connection of coordination polyhedron. In this paper we report high pressure studies on Li_2CuO_2 using diamond anvil cell (DAC) with angle dispersive X-ray diffraction (ADXD) of synchrotron radiation and with electrical conductivity measurements. The experimental results are compared with first-principle calculations.

2. Experimental

The Li_2CuO_2 sample was synthesized by conventional solid state reaction from high purity $LiOH \cdot H_2O$ (AR, $\geq$95%) and CuO (AR, $\geq$99%). Stoichiometric ratio of reagents were mixed and grounded in an agate mortar. The mixture was heated at 420 °C for 8 h, and then calcined at 700 °C for 36 h in air. The product obtained is yellow–brown polycrystalline powder that is very sensitive to moisture and turns to dark brown quickly in air with trace of CuO appeared in the X-ray diffraction pattern. Therefore the sample has to be preserved in a dry box.

In-situ high-pressure ADXD experiments were carried out at room temperature using a DAC at both HPCAT of advanced photon source (APS) and on the X17C beam line at National Synchrotron Light Source (NSLS) at the Brookhaven National Laboratory. An incident beam with a wavelength of 0.4066 Å was collimated to a size of 10 and 50 μm in diameters, respectively. The culet of the diamond anvils was 400 μm in diameter. The Li_2CuO_2 sample was finely ground and loaded into a Φ150 μm hole in a T301 stainless steel gasket which had been pre-indented to a thickness of ~30 μm from the initial thickness of 250 μm. Silicon oil was used as a pressure transmitting medium. The applied pressure of the DAC was monitored by the position shift of the luminescence line R_2 [24] from a small ruby chip placed around the sample. Diffraction patterns were recorded on a Fuji image plate then analyzed by integrating the image in azimuth as a function of 2θ using the program FIT2D [25].

The spectra of ADXD were refined using the program EXPGUI [26] for GSAS [27]. Program Treor90 [28] was used to index the high pressure patterns. A Pawley refinement [29] was then performed to investigate the potential structure of high pressure phase. An in-situ four-point resistance measurement was

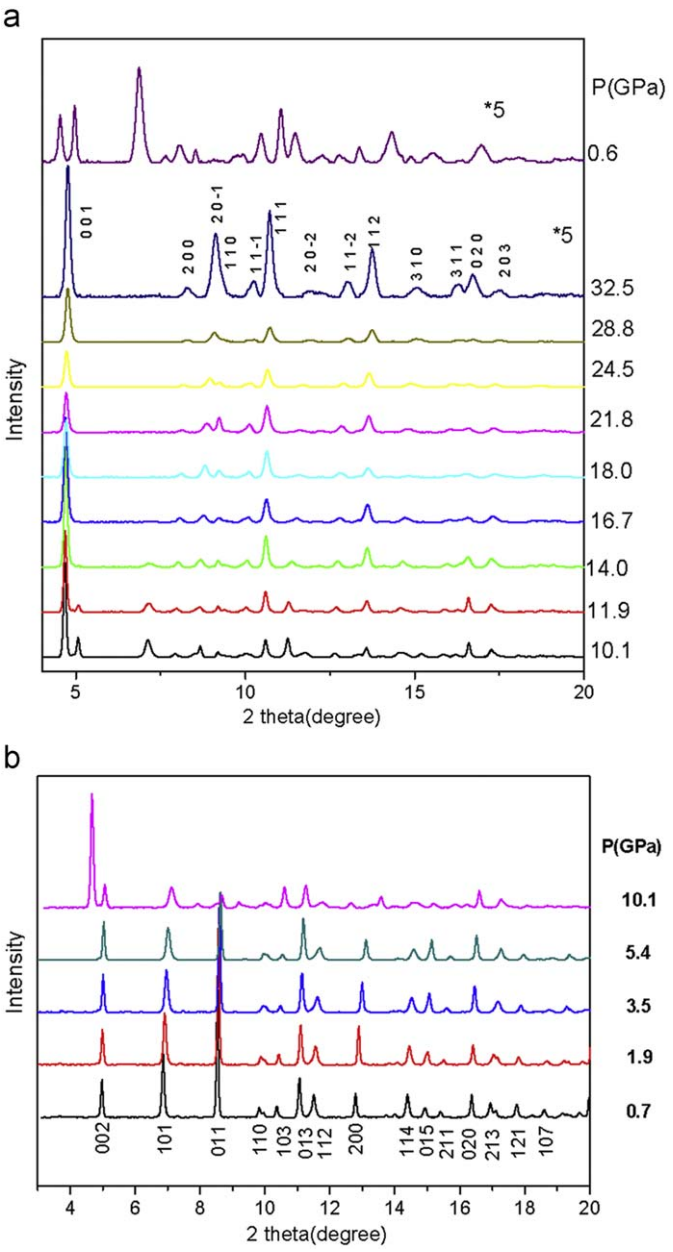

Fig. 2. The X-ray diffraction patterns of the Li_2CuO_2 sample under various pressures at room temperature. The intensities of spectra at 32.5 and 0.6 GPa after releasing pressure are expanded by five times for clarity.

also performed at high pressure and at room temperature using a DAC.

The first principle calculations were conducted using local density approximation (LDA) $+U$ implemented in VASP package [30] with spin–polarization. The on site Coulomb interaction U is set to be 7 eV that will not affect the result of calculations on enthalpy. The spin–orbital coupling is ignored in our calculations since the orbital moment is usually quenched for 3d transition elements. The projector augmented-wave (PAW) pseudo-potentials [31] with a 750 eV plane-wave cutoff are used and the criterion for convergence is 10^{-5} eV/cell.

3. Results and discussion

The X-ray diffraction spectra of Li_2CuO_2 at room temperature under a pressure range of 0.7∼32.5 GPa are shown in Fig. 2. Below 5.4 GPa, all diffraction peaks could be indexed to the orthorhombic structure of Li_2CuO_2 (phase I). The diffraction peaks shift toward higher angle side as the pressure increases. Sets of new peaks appear in the pressure range from 5.4 to 18.9 GPa, likely arising from a new phase. As pressure increases, the intensity of the new peaks gets stronger while the initial diffraction peaks of Li_2CuO_2 phase I become weakening and finally disappear under pressure above 18.9 GPa. The diffraction pattern at higher pressure shows the stabilization of the new phase (named phase II) at least up to 32.5 GPa.

As described above, the phase I structure of Li_2CuO_2 remains stable under pressure below 5.4 GPa. The lattice and atomic parameters were obtained by refining the X-ray diffraction data using the GSAS program. The result shown in Fig. 3(a) indicates an anisotropy behavior of Li_2CuO_2 with smallest compressibility along b axis. This is in agreement with a high pressure study on $LiCuO_2$ showing a smaller compressibility along the CuO_2 chain [32]. The bulk modulus was obtained by fitting the experimental data to the Birch–Murnaghan equation of state (EOS). Assuming the first-order derivative $B_0' = 4$, we get $B_1 = (78.2 \pm 3.1)$ GPa. The Cu–O distance decreases from 1.952 Å (at 0.7 GPa) to 1.881 Å (at 5.4 GPa) as shown in Fig. 3(b). Pressure induced Cu–O–Cu angle changing from ∼94° at 0.7 GPa to 97.4° at 5.4 GPa since the lattice parameter along c axis shrinks faster than that of ab plane. According to Goodenough–Kanamori–Anderson rule [12–14], such an increase in Cu–O–Cu bond angle would magnify the evolution of spin interaction and lead to a growth of AFM interaction in the CuO_2 chain.

The spectra at 28.8 GPa was selected for solving the structure of high pressure phase (II) since the transformation is completed under this pressure and the intensity remains good enough for structure refinement. Fourteen diffraction peaks were picked up in the range of 3–18° of 2θ angle. All the peaks could be well

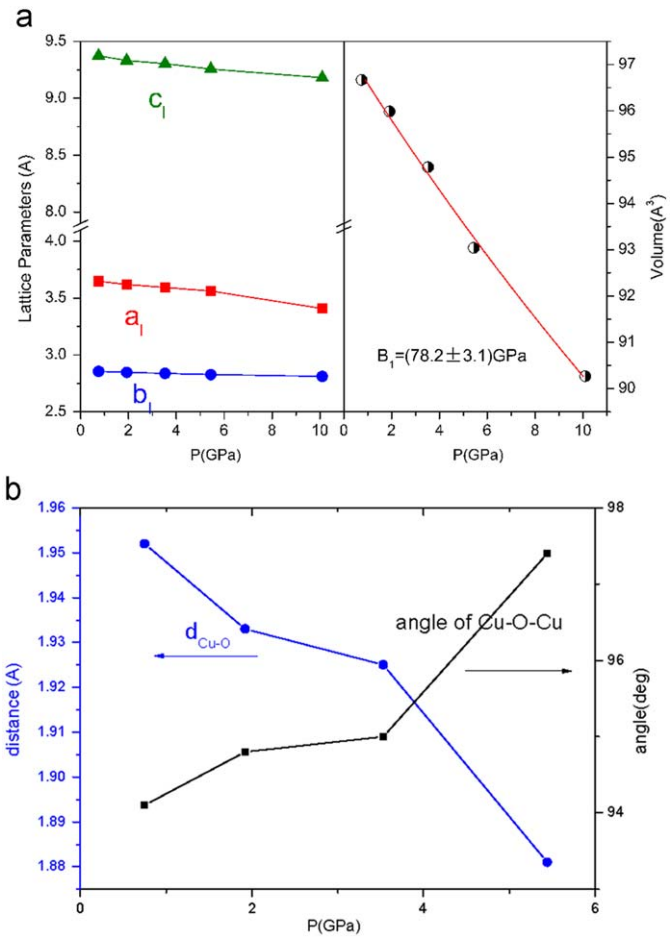

Fig. 3. (a) Pressure dependence of lattice parameters and volume of phase I. (b) Pressure dependence of Cu–O distance (blue) and angle (black) of Cu–O–Cu in Li_2CuO_2 phase I. The error bars are relatively small and within the symbol sizes. (For interpretation of the references to colour in this figure legend, the reader is referred to the web version of this article.)

Table 1
Structure parameters derived from the Rietveld refinement for Li_2CuO_2 high pressure phase at 28.8 GPa.

a (Å)	b (Å)	c (Å)	β (deg)	V (Å^3)
5.6346(22)	2.7853(8)	4.9233(18)	97.128(25)	76.669(56)
		x	y	z
Li	(4i)	0.1921(33)	0	0.1182(34)
Cu	(2d)	0	0.5	0
O (4i)	(4i)	0.1316(18)	0	0.7583(14)
	R_{wp}=1.36%		R_p=1.14%	

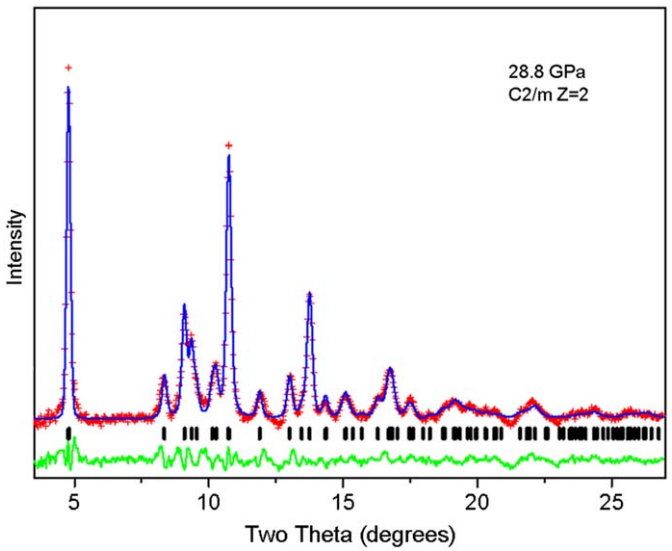

Fig. 4. The Rietveld refinement of XRD data at 28.8 GPa using GSAS program, with a=5.6334(25) Å, b=2.7801(11) Å, c=4.9133(13) Å, β=97.017(39)°, Z=2, S.G. $C2/m$. R_{wp}=1.36%, R_p=1.14%. The red crosses are the experimental data points; the blue line is the calculated pattern. The vertical bars indicate the positions of Bragg diffractions. The green line represents the residual (exp. subtracts cal.) from the fit. (For interpretation of the references to colour in this figure legend, the reader is referred to the web version of this article.)

indexed to a monoclinic structure with a=5.635 Å, b=2.785 Å, c=4.923 Å, β=97.128°, V=76.669 Å^3, Z=2 using Treor90 [28]. According to the extinction rules, Pawley refinement gave three possible space groups as Cm, $C2/m$ and $C2$ for this monoclinic structure, respectively. Among the three candidate space groups, we chose $C2/m$ as the space group of phase II since it has more symmetric elements than the other two. We have probed all the allowed occupations of copper and oxygen atoms. It turns out that a structural solution could be obtained when Cu atoms occupy 2d positions (0, 1/2, 1/2) as oxygen and lithium atoms locate in the 4i positions (x, 0, z), respectively. The detailed atomic parameters were derived from Rietveld refinement using the GSAS program as listed in Table 1. Fig. 4 shows the fitting result of Rietveld refinement under 28.8 GPa. A reasonable R_{wp} factor was obtained.

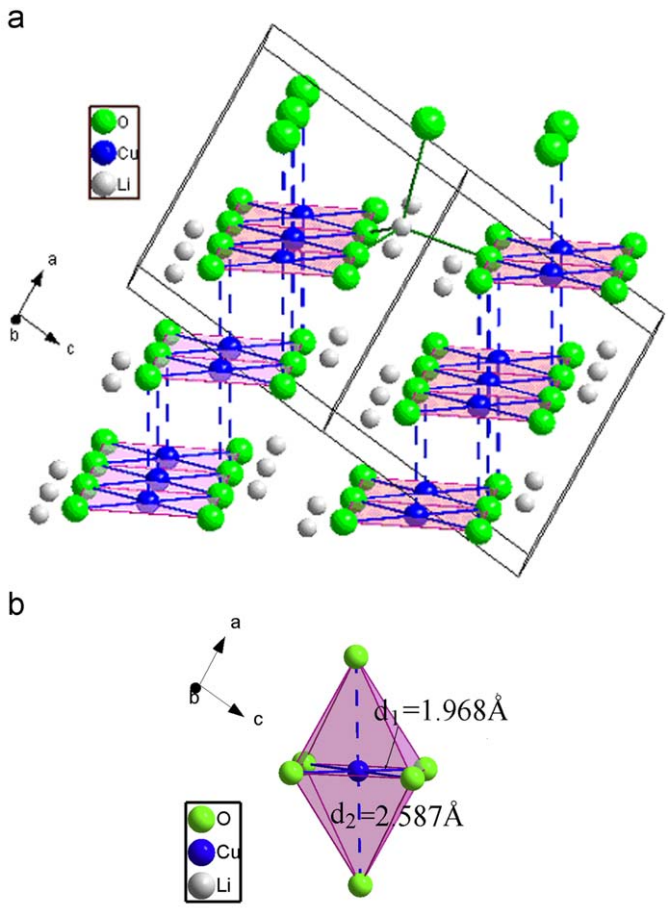

Fig. 5. Schematic view of the potential structure of high pressure or phase (II) of Li_2CuO_2 at 28.8 GPa, S.G $C2/m$ (no. 12) indicating the outlined unit cell as well as the Cu–O octahedron coordination.

Applying this structure to other ADXD data, we found that all the diffraction patterns obtained under pressure above 18.9 GPa could be refined as a single phase, an indication of the feasibility of the structure model. The crystal structure of the phase II is shown in Fig. 5. The CuO_2 chain runs along the b axis in phase I. At high pressure, a distortion occurred in the stacking of Cu chains through the relative approaching each other of the edge sharing CuO_2 chains. The distortion changes the coordination number of Cu ions from four-square in ambient phase to six-octahedron in high pressure phase. This is consistent with the general trend that the coordination number increases as pressure increasing, such as observed in $MgSiO_3$ [1]. The approaching of apical oxygen to [CuO_4] square results in increased Coulomb repulsion within the in-planar oxygen, leading to the expansion of Cu–O distance in the square comparing to the phase I. Table 2 shows the evolution of CuO_4 square both in Cu–O distances and Cu–O–Cu bond angles as the apical oxygen comes closer in high pressure. In contrast to the change of coordination of Cu^{2+} ions, the coordination polygons of Li^+ ions keep in tetrahedral during the structure transition except for a variation in Li–O distances as shown in Table 2.

To further understand the structure of the high pressure phase, enthalpies of both phase I and II under different pressures were calculated by the first-principle calculation [31]. The result is shown in Fig. 6, indicating a structural transition occurs under pressure about 6.5 GPa. The monoclinic phase II will be more stable than the orthorhombic phase I under pressure above 6.5 GPa in terms of energy. The calculated transition pressure fits reasonably well with our experiment, which further supports the structure refinement.

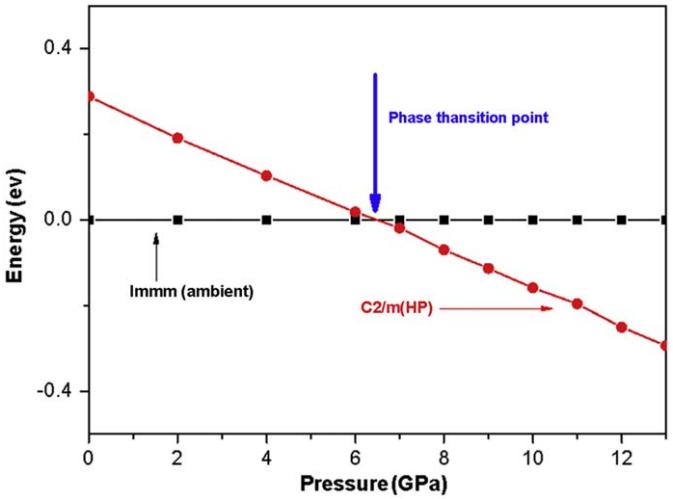

Fig. 6. The enthalpy for monoclinic phase (II) (the red line) as a function of pressure, referenced to the enthalpy of the orthorhombic phase (I) (the black line). The calculation indicates that the phase I→II transition starts at ~6.5GPa. (For interpretation of the references to colour in this figure legend, the reader is referred to the web version of this article.)

Table 2
The Li–O and Cu–O distances and Cu–O–Cu angles along the edge sharing chains at high pressure (phase II).

Pressure (GPa)	Distance (Å)		Bond angle (deg)	Distance (Å)		
	Cu–O		Cu–O–Cu	Li–O		
18.9	1.965(5)	2.695(12)	91.28(30)	1.838(21)	1.971(31)	1.810(17)
21.8	1.967(7)	2.639(19)	90.80(40)	1.811(33)	2.070(40)	1.758(22)
24.5	1.9628(5)	2.6166(10)	90.897(30)	1.7903(4)	2.0004(8)	1.7895(4)
28.8	1.968(5)	2.565(11)	90.22(29)	1.763(16)	1.993(23)	1.774(12)
32.5	1.956(4)	2.493(9)	90.66(24)	1.915(23)	2.091(25)	1.671(13)

The XRD pattern shows the coexistence of both phase I and II as the pressure released, which implies that phase II is metastable at ambient pressure, i.e. the pressure-induced phase transition is reversible. The pressure dependence of lattice parameters and volumes of the phase II are shown in Fig. 7. A volume collapse appeared at 10.1 GPa with a decreasing ratio of 7% comparing with orthorhombic phase I. The bulk modulus of phase II is (107.4 ± 3.3) GPa that is obtained by fitting the experimental data with Birch–Murnaghan equation of state (EOS) with $B_0' = 4$. The bulk modulus of the phase II (107.4 ± 3.3) GPa is much higher than that of the phase I, (78.2 ± 3.1) GPa, indicating a stiffer and more compact structure under high pressures. It is also observed that in phase II Cu–O–Cu bond angle decreases to 90.7° at 32.5 GPa. The near 90° Cu–O–Cu angle in phase II enforces the ferromagnetic interaction according to Goodenough–Kanamori–Anderson rule [12–14]. Therefore the intra-chain spin-order of Li_2CuO_2 also tends to be ferromagnetic as the case in the ambient phase.

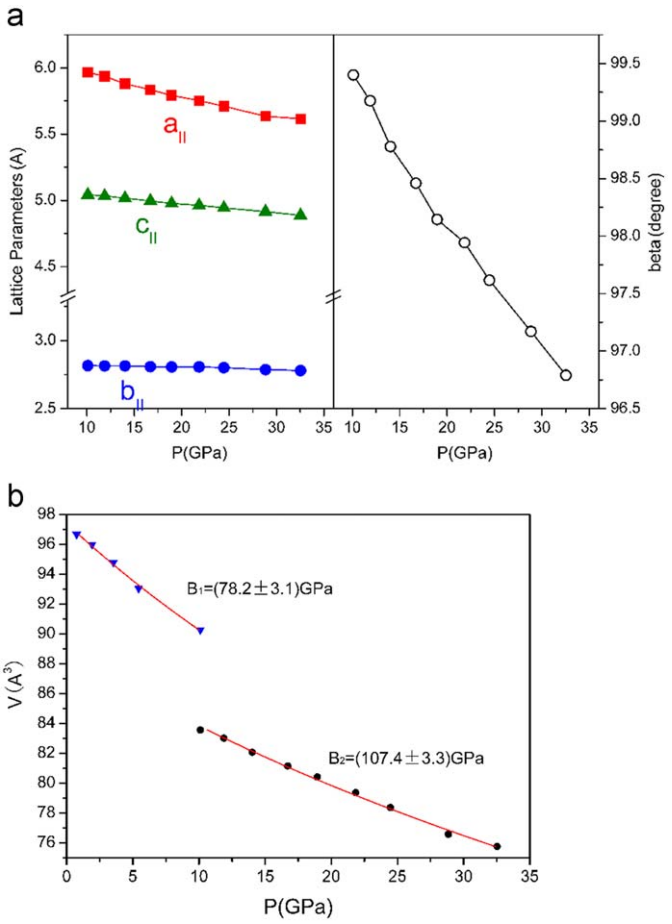

Fig. 7. (a) Pressure dependence of lattice parameters of phase II. (b) Volume vs. pressure data for phase I (triangles) and phase II (circles) of Li_2CuO_2. The solid lines represent the EOS fitted of each phase.

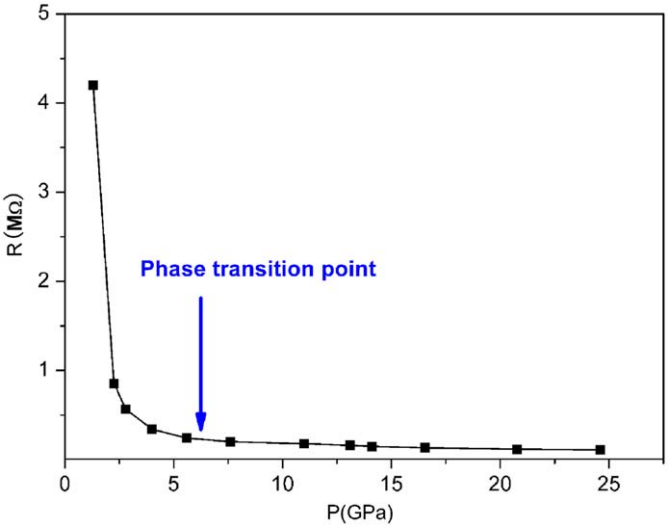

Fig. 8. The resistance vs. pressure of Li_2CuO_2 at room temperature.

In phase I, the inter-chain spin coupling is weak with $T_N \sim 9$ k which could be easily destroyed by temperature. In our experiment, phase II has a shorter distance between parallel CuO_2 chains (perpendicular to the CuO_4 plaque) comparing with the phase I, which indicates a stronger inter-chain coupling, and might lead to different inter-chain spin-order. The first principle calculations indeed indicated that the phase II is a C type anti-ferromagnetic insulator for pressure < 150 GPa (by Li et al., to be submitted). A sharp resistance drop around 6 GPa followed with a flat slope at higher pressure (as shown in Fig. 8) implies a phase transition, in consistent with the X-ray diffraction measurements. Taking into account the result of the high pressure X-ray diffraction experiment, it is possible that the relatively smaller resistance of phase II is caused by a stronger inter-chain coupling due to the decreased distance between parallel CuO_2 chains. The relatively weak pressure dependence of the resistance in phase II is possibly due to the more compact structure and large bulk modulus that makes the electronic structure of high pressure phase more sustainable upon compression.

4. Conclusions

A structural phase transformation was observed in Li_2CuO_2 at pressure above 5.4 GPa. The structure of this new phase is modeled to be a monoclinic lattice with a potential space group $C2/m$. Increasing pressure results in coordination numbers of Cu increasing from four (square) to six (octahedron). This dimensionality change leads to higher electrical conductivity of the high pressure phase, while the spin orientates in a C type anti-ferromagnetic ordering. The experimental observations are well supported by the first principle calculations.

Acknowledgments

We thank Quanzhong Guo and other NSLS stuff for technical supports during experiments on beamline X17C at NSLS. This work was financially supported by NSF and MOST of China through the research projects. The experiments at X17C, NSLS were partially supported by COMPRES. HPCAT is supported by DOE-BES, DOE-NNSA, NSF, and the W.M. Keck Foundation. APS is supported by DOE-BES, under Contract no. DE-AC02-06CH11357.

References

[1] M. Murakami, K. Hirose, K. Kawamura, N. Sata, Y. Ohishi, Science 304 (2004) 855.
[2] M. Uehara, T. Nagata, J. Akimitsu, H. Takahashi, N. Mori, K. Kinoshita, J. Phys. Soc. Jpn. 65 (1996) 2764.
[3] T. Nagata, M. Uehara, J. Goto, et al., Physica C 282–287 (1997) 153.
[4] H. Rosner, R. Hayn, S.L. Drechsler, Physica B 261 (1999) 1001.
[5] Y. Mizuno, T. Tohyama, S. Maekawa, Phys. Rev. B 60 (1999) 6230–6233.
[6] D. Mertz, R. Hay, I. Opahle, H. Rosner, Phys. Rev. B 72 (2005) 085133.
[7] H. Arai, S. Okada, Y. Sakurai, J. Yamaki, Solid State Ionics 106 (1998) 45–53.

[8] N. Tanaka, M. Suzuki, K.J. Motizuki, Magn. Magn. Mater. 196–197 (1999) 667.
[9] Y.J. Kim, J.C. Hill, F.C. Chou, D. Casa, T. Gog, C.T. Venkataraman, Phys. Rev. B 69 (2004) 155105.
[10] R. Hoppe, H.Z. Rieck, Anorg. Allg. Chem. 379 (1970) 157–164.
[11] H. Völlenkle, A. Wittmann, H. Nowotny, Monatsh. Chem. 98 (1967) 1352.
[12] H.J. Kanamori, Phys. Chem. Solids 10 (1959) 87–98.
[13] J.B. Goodenough, Magnetism and the Chemical Bond, Interscience Publisher, New York, 1963.
[14] P.W. Anderson, in: G.-T. Rado, H. Suhl (Eds.), Magnetism, vol. I, Academic Press, New York, 1963.
[15] T. Siegrist, L.F. Schneemeyer, S.A. Sunshine, J.V. Waszczak, R.S. Roth, Mater. Res. Bull. 23 (1988) 1429–1438.
[16] S. Ebisu, T. Komatsu, N. Wada, T. Hashiguchi, P. Kichambare, S. Nagata, J. Phys. Chem. Solids 59 (1998) 1407.
[17] U. Staub, B. Roessli, A. Amato, Physica B Condens. Matter 289–290 (2000) 299.
[18] F. Sapiña, J. Rodríguez-Carvajal, M.J. Sanchis, R. Ibáñez, A. Beltrán, D. Beltrán, Solid State Commun. 74 (1990) 779–784.
[19] S. Giri, H. Chudo, H. Nakamura, H.J. Shiga, J. Alloys Compd. (2001) 61–64.
[20] L.C. Ming, S.R. Shieh, A. Jayaraman, S.K. Sharma, Y.H. Kim, J. Phys. Chem. Solids 60 (1) (1990) 69–87.
[21] A. Yoshiasa, C. Yagyu, T. Ito, T. Yamanaka, T.Z. Nagai, Anorg. Allg. Chem. 626 (1) (2000) 36–41.
[22] P. Dera, A. Jayaraman, C.T. Prewitt, S.A. Gramsch, Phys. Rev. B 65 (2002) 134105.
[23] M. Nishi, O. Fujita, J. Akimitsu, K. Kakurai, Y. Fujii, Phys. Rev. B 52 (1995) R6959.
[24] H.K. Mao, J. Xu, P.M. Bell, J. Geophys. Res. 91 (B5) (1986) 4673–4676.
[25] A.P. Hammersley, FIT2D, 12_077(2004), Reference Manual V6.0, European Synchrotron Radiation Facility, Grenoble, France.
[26] B.H. Toby, J. Appl. Crystallogr. 34 (2001) 210–213.
[27] R.B. Von Dreele, J. Appl. Crystallogr. 30 (1997) 517–525.
[28] C. Dong, J. Appl. Crystallogr. 32 (1999) 838.
[29] G.S. Pawley, J. Appl. Crystallogr. 14 (1981) 357–361.
[30] 〈http://cms.mpi.univie.ac.at/vasp/〉.
[31] P.E. Blöchl, Phys. Rev. B 50 (1994) 17953–17979.
[32] W. Utsumi, K. Imai, M. Koike, H. Takei, T. Yagi, H. Takahashi, N. Môri, J. Solid State Chem. 107 (2) (1993) 507–512.